

Snell's law in multirefringent systems

József Cserti,¹ Áron Holló,¹ and László Oroszlány²

¹*Department of Physics of Complex Systems, ELTE Eötvös Loránd University, H-1117 Budapest, Pázmány Péter sétány 1/A, Hungary*

²*Department of Physics of Complex Systems, ELTE Eötvös Loránd University, H-1117 Budapest, Pázmány Péter sétány 1/A, Hungary
Wigner Research Centre for Physics, H-1525, Budapest, Hungary*

In anisotropic crystals, Maxwell's equations permit only birefringence for the propagation of light. Notwithstanding, multirefringent systems comprising more than two propagating modes exist, such as in electron optics and photonic crystals. It has been demonstrated that in such systems, the propagation of waves in the short wavelength limit results in the formation of anomalous caustics. To calculate these caustic curves, we generalized Snell's law valid for reflection and refraction in multirefringent systems possessing more than one propagating mode. The emergence of anomalous caustics in the wave function patterns obtained from rigorous quantum mechanical calculations in electron-optical systems is confirmed. These calculations were performed on electron scattering from circularly gated potential regions applied to multilayer rhombohedral graphene. Our results may generate further work to explore more complex phenomena in multirefringent systems.

Introduction.— Birefringence, or double refraction related to crystal anisotropy is a well-known phenomenon in optics [1]. In the most general case, due to Maxwell's equations, in anisotropic, non-magnetic, dielectric crystals, only birefringence is allowed. As it is well known, birefringence gives rise to a wide range of optical phenomena and several applications, see e.g., [2]. Recently, bi-reflection of spin waves has been observed experimentally in magnonics system as well [3].

Photonic crystals fabricated on the scale of the optical wavelength opened a new field in optics [4]. For instance, in contrast to birefringence in dielectric crystals, multirefringence can be observed in trirefringent photonic crystal waveguides [5]. A theoretical study of trirefringence at the surface of metamaterials has also been reported recently [6]. The existence of triple refraction was proposed in nonlinear metamaterials as well [7].

Non-trivial wave propagation in materials with negative refractive indices gives rise to another exotic phenomenon. The existence of negative refraction indices has been theoretically proposed by Veselago and Pendry [8, 9] have been experimentally realized in photonic crystals [10–12] and in acoustic materials [13]. Research in this direction was initiated by the seminal work of Cheianov et al., proposing the realization of negative refractive index for electrons in graphene [14]. Electron focusing phenomenon in graphene has been further studied in Refs. [15–24] and also in other two-dimensional (2D) electronic systems [25–29]. A perspective view of the realization of a 2D Dirac fermion-based microscope has now been considered [30]. In a recent publication, electron quantum optics in graphene has been reviewed [31].

In geometrical optics, classical ray approximation is the short-wavelength limit of electromagnetic theory. The envelope of a ray family is called the caustic. In the ray approximation, the density of the wave function

patterns along the caustics is singular, thus they can be well seen even for finite wavelengths. Caustics have been studied extensively in the past (for a review see e.g. Berry and Upstill [32] and Berry [33]).

In this paper, we demonstrate that multirefringence, in contrast to birefringence as commonly observed in dielectric crystals, results in additional complexity. To this end, we consider the refraction of parallel rays incident on a circular region with more than two different refractive indices in ray approximation. As an illustration in Fig. 1 we depict characteristic features due to multirefringence in a region with three different refractive indices. Two types of caustic curves of the reflected rays can be formed inside the region interest: (i) *regular* caustics, where all rays are related to reflections with the same refractive index, (ii) *anomalous* caustics (as we shall call them from now on), when the reflections inside the region involve more than one refractive index. The former is the usual caustics observed in a material with a single refractive index while the latter can only exist in multirefringent systems. From now on, we use the language of electron optics. However, our results can easily be extended to systems such as photonic crystals or acoustic waves in sonic crystals.

Multirefringence.—We now outline the characteristic features of multirefringence in multi-band systems. Consider the propagation of free electrons through a flat interface in such systems. Assume that the number of plane wave solutions of the Schrödinger equation in the left (L) and the right-hand (R) sides of the interface with wave vector \mathbf{k} are N_L and N_R ($N_{L/R} > 1$) component spinor wave functions and the corresponding energy eigenvalues are $E_j^{(L/R)}(\mathbf{k})$, where $j, l = 1, 2, \dots, N_{L/R}$. The system possesses $N_{L/R}$ number of bands at the two sides of the interface. Here we assume that the system has isotropic band structures. In this case, on both sides of the interface, the group velocities $\mathbf{v} = \partial_{\mathbf{k}} E(\mathbf{k})/\hbar$ are parallel

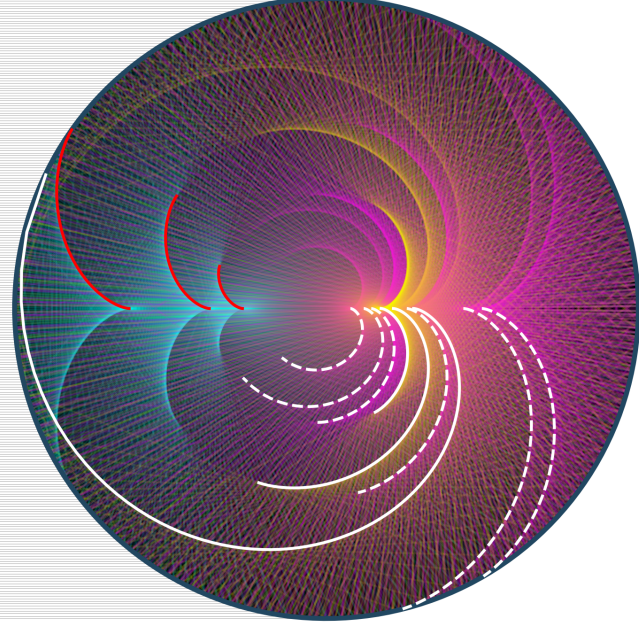


FIG. 1: Incident parallel rays from left (thin black solid lines) are refracted in three different directions (cyan-colored rays) at the circular surface, due to three different refractive indices of the region. The envelope of these rays, marked by red solid lines correspond to regular caustics. These rays are reflected inside the circular region either without changing the refractive index (yellow-colored rays) or with an altered refractive index (magenta-colored rays). The envelopes of the yellow rays, marked by white solid lines are further regular caustics. The envelopes of rays with magenta color, highlighted by dashed white lines, are anomalous caustics.

with the wave vector. To elucidate electron optical phenomena, one first needs to consider ray optics on a flat interface as depicted in Fig. 2. For a given energy E the allowed wave vectors $\mathbf{k}_j^{(L/R)}$ at the left and right side of the interface, respectively are the solutions of the equation $E_j^{(L/R)}(\mathbf{k}) = E$. An incident ray with a wave vector $\mathbf{k}_j^{(L)}$ in general will be reflected/refracted into $N_{L/R}$ number of rays with corresponding wave vectors $\mathbf{k}_m^{(L/R)}$.

Generalized Snell's law.— For a given incident angle $\phi_j^{(L)}$ the reflection angles $\chi_m^{(L)}$ and the refracted angles $\phi_l^{(R)}$ can be determined from Snell's law which follows from the conservation of the y components of the incident/reflected/refracted wave vectors at the flat interface:

$$k_j^{(L)} \sin \phi_j^{(L)} = k_m^{(L)} \sin \chi_m^{(L)}, \quad j, m = 1, 2, \dots, N_L \quad (1a)$$

$$k_j^{(L)} \sin \phi_j^{(L)} = k_l^{(R)} \sin \phi_l^{(R)}, \quad l = 1, 2, \dots, N_R \quad (1b)$$

where $k_{j,m}^{(L)} = |\mathbf{k}_{j,m}^{(L)}|$ and $k_l^{(R)} = |\mathbf{k}_l^{(R)}|$ are the magnitudes of the corresponding wave vectors. These equations can be regarded as a generalization of Snell's laws valid

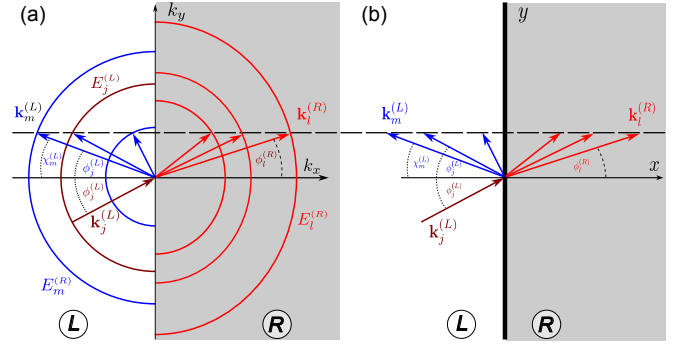


FIG. 2: Multiple reflections and refractions for isotropic band structures. (a) In \mathbf{k} -space the incident wave $\mathbf{k}_j^{(L)}$ (brown arrow) from the left side (L) of the interface will be reflected (blue arrows) and refracted (red arrows) with wave vectors $\mathbf{k}_m^{(L)}$ and $\mathbf{k}_l^{(R)}$ at the left and right sides of the interface (R), respectively. The constant energy surfaces (circles in 2D) are labeled by $j, m = 1, 2, \dots, N_L$ and $l = 1, 2, \dots, N_R$ at the left and right-hand sides of the interface, respectively. For clarity in the figure, only three bands are shown on both sides. (b) shows the corresponding real-space trajectories of the reflected/refracted waves.

for reflections and refractions in multirefringent systems. Note that the same equations of Snell's law are valid for reflected and refracted elastic waves at the boundary between two different elastic media [34].

To demonstrate interband scattering highlighted above, we now consider one incoming plane wave (propagating from left to right as in Fig 1.) outside the circular potential region. For a given energy E , the sets of the allowed wave numbers inside and outside the potential region are denoted by $\mathbb{K}^< = \{k_1^<, \dots, k_N^<\}$ and $\mathbb{K}^> = \{k_1^>, \dots, k_N^>\}$, respectively. For simplicity, we assumed that the number of wave numbers inside and outside are the same N . Naturally, the wave number k_0 of the incident wave is taken from the set $\mathbb{K}^>$. We now define a set of refractive indices \hat{n} corresponding to the possible wave numbers inside the circular potential (the set $\mathbb{K}^<$) as follows

$$\hat{n} = \left\{ \frac{k}{k_0} \mid k \in \mathbb{K}^< \right\} \equiv \{n_1, \dots, n_N\}. \quad (2)$$

Note that for anisotropic systems, the direction of the group velocities which is perpendicular to the constant energy surface, is not necessarily parallel to the wave vector. In contrast to the dielectric crystals where only birefringence exists, in multi-band systems with $N > 2$ number of bands, multirefringence can arise. Another intriguing feature of electron optics, realized for instance in graphene p-n junctions, is the feasibility of a negative refractive index. [20–23]. In this case, we have $\mathbf{v}(\mathbf{k}) \cdot \mathbf{k} < 0$.

Anomalous caustics.—To describe the formation of caustics in multi-band systems we consider a specific geometrical arrangement shown in Fig 1. Inside the circular

region, the refracted and the reflected rays of the incoming ray are straight lines called cords and numbered by p corresponding to $p - 1$ reflections. The coordinates of the vertices \mathbf{V}_i from which the rays are reflected at the circle of radius R , i.e., the endpoints of the cords can be parameterized as follows $\mathbf{V}_i = R[\cos \varphi_i, \sin \varphi_i]^T$ for $i = 0, 1, \dots, p$, where $\varphi_0(\alpha) = \pi - \alpha$, and $\varphi_i(\alpha) = \pi - \alpha \pm \sum_{j=1}^i [\pi - 2\chi_j(\alpha)]$ for $i = 1, 2, \dots, p$, and χ_j are the reflection angles at the vertex \mathbf{V}_j which according to Eqs. (1) discussed above satisfy our generalized Snell's law

$$\sin \alpha = n_1 \sin \chi_1, \quad (3a)$$

$$n_j \sin \chi_j = n_{j+1} \sin \chi_{j+1}, \quad \text{for } j = 1, 2, \dots, p, \quad (3b)$$

where α is the incident angle of the incoming ray. The $+$ and $-$ signs in the definition of $\varphi_i(\alpha)$ correspond to the negative and positive refractive index, respectively, and the angles φ_i are measured, as usual from the positive x axis. However, in the absence of interband scattering, these angles are the same as they should be for a system with a single refraction index.

Typical ray paths with reflection angles χ_j ($j = 1, 2, 3$) are shown in Fig. 3 for positive and negative refractive index. In this figure the reflection angles χ_j are different

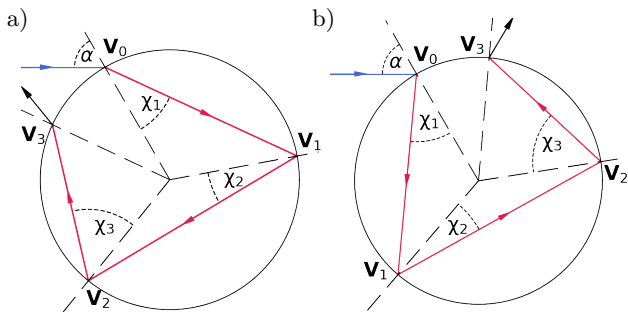


FIG. 3: Typical reflections of a ray inside the circular region for positive (a) and negative (b) refractive indices in case of $N = 3$ number of bands and $p = 3$ chords.

owing to the different wave numbers of the reflected rays. Therefore, each cord forms an anomalous caustic curve as the incident angle α varies and it can be calculated using differential geometry [35]. We find (see Supplemental Material [36]) the parametric equation of the regular and anomalous caustic curves corresponding to the p th chord as a function of α :

$$\mathbf{r}_c^{(p)}(\alpha) \equiv \begin{bmatrix} x_c^{(p)}(\alpha) \\ y_c^{(p)}(\alpha) \end{bmatrix} = \frac{\mathbf{V}_{p-1} \dot{\varphi}_p + \mathbf{V}_p \dot{\varphi}_{p-1}}{\dot{\varphi}_{p-1} + \dot{\varphi}_p}, \quad (4)$$

where the dot denotes the derivative with respect to α . Thus, $\dot{\varphi}_i = \frac{\partial \varphi_i}{\partial \alpha} = -1 \mp 2 \sum_{j=1}^i \dot{\chi}_j$, and from the Snell's law (3) we have $\dot{\chi}_j = \cos \alpha / (n_j \cos \chi_j)$.

To highlight the characteristic features of multirefringence discussed above, we present a full quantum mechanical solution of the scattering problem of electrons

impinging on a circular potential region, shown in Fig. 1. To this end, we carried out the calculations in rhombohedral graphene multilayers, widely studied in the literature [37–41]. The Hamiltonian of N -layer rhombohedral graphene has N different positive energy electronic bands. Consequently, for a given energy there can, in general, be N different wave numbers in one valley for states propagating in one direction. The details of the quantum mechanical calculations of the scattering problem are given in the Supplemental Material [36].

The calculations can be regarded as an extension of that carried out for single and bilayer graphene [15–18].

As an example of multirefringence, in Fig. 4 we show the wave function pattern obtained from our fully quantum mechanical calculations for rhombohedral graphene with $N = 3$ and $N = 4$ layers, together with the caustics curves calculated from our analytic formula (4). As can be seen, the caustic curves are well separated, and fit well to the intensity maxima of the calculated wave functions (for symmetry reasons only half of the caustic curves are shown to compare with the numerical results). Since caustics are related to geometrical optics, we cannot expect full agreement with the quantum mechanical result because the classical result does not take into account the quantum mechanical interference effect, and reflection and transmission amplitudes at the circular potential. Thus in the figure, we only highlight caustic curves that are well-visible in the wave function pattern. The scattered wave function pattern is calculated in the semiclassical regime, i.e., in short wavelength limit, $kR \gg 1$ for incoming and refractive waves, where R is the radius of the circular region of the scattering potential. In general, it is clear that for the p th caustics (corresponding to the p th chord) in a multirefringent system with N number of refraction indices, the number of regular caustics is N , and the number of anomalous caustics is $N^p - N$. This is well illustrated in Fig. 1, where there are three regular caustics for all p , and for $p = 2$ six anomalous caustic curves can be seen, in the case of $N = 3$.

The locations of the cusps in the caustic curves, $(x, y) = (x_{\text{cusp}}^{(p)}, 0)$ can be derived from Eq. (4) in the limit of $\alpha \rightarrow 0$. For regular caustics, the result is the same as that obtained in Ref. 15 for arbitrary p :

$$x_{\text{cusp}}^{(p)} = \frac{(-1)^p}{|n| - 1 + 2p} R, \quad (5)$$

where n is the refractive index of the circular region. This expression, for the location of the cusps, can be generalized to an arbitrary number of refractive indices encompassing regular and anomalous caustic curves. As an example of two different refractive indices the locations

of the two cusps with $p = 2$ chords we obtained

$$x_{\text{cusp}}^{(2)} = \frac{|n_1|}{|n_1| + 2|n_2| + |n_1||n_2|}R, \quad \text{and} \quad \{n_1 \leftrightarrow n_2\}. \quad (6)$$

Note that as a consequence of Snell's law (3) for reflection, the positions of the cusps are not the same for the exchange of the two refractive indices. Similar expressions can be derived for $p > 2$.

Using Eqs. (5) and (6) the corresponding cusp positions are listed in Table I for $N = 3$ and $N = 4$. Note that in this table for regular (anomalous) caustics the refractive indices are the same (different). One can see from the table that these cusps are well distinguishable.

$x_{\text{cusp}}^{(p=1)}$		$x_{\text{cusp}}^{(p=2)} (N=3)$		$x_{\text{cusp}}^{(p=2)} (N=4)$	
$N = 3$	$N = 4$	$n_1 \rightarrow n_2$	$x_{\text{cusp}}^{(p=2)}$	$n_1 \rightarrow n_2$	$x_{\text{cusp}}^{(p=2)}$
-0.44	-0.45	-0.54 \rightarrow -1.25	0.15	-0.48 \rightarrow -1.24	0.14
-0.54	-0.51	-0.86 \rightarrow -1.25	0.19	-0.66 \rightarrow -1.24	0.17
-0.65	-0.60	-1.25 \rightarrow -1.25	0.24	-0.96 \rightarrow -1.24	0.21
-	-0.68	-1.25 \rightarrow -0.86	0.31	-1.24 \rightarrow -1.24	0.24
-	-	-0.86 \rightarrow -0.54	0.36	-1.24 \rightarrow -0.96	0.29

TABLE I: The locations of the cusps $x_{\text{cusp}}^{(p=1)}$ for $p = 1$ chords, and $x_{\text{cusp}}^{(p=2)}$ for $p = 2$ chords of the caustic curves shown in Fig. 4 in case of $N = 3$ and $N = 4$ layers. The locations are in units of R . For $p = 1$ there are only regular caustic curves. In the case of $p = 2$ the two refractive indices n_1 and n_2 are the same for regular caustics, while for different n_1 and n_2 the caustics are anomalous (red numbers).

We would like to emphasize that the results for caustic curves, cusp locations, and their agreement with the quantum mechanical solution are in alignment with previous studies on bilayer graphene [16]. We present further evidence of this in the Supplemental Material [36].

Conclusions.— We studied the wave propagation in materials with multiple propagating modes. We generalized Snell's law for reflections and refractions in the short wavelength limit corresponding to the geometrical optics-like treatment. We demonstrated that interband scattering leads to the formation of *anomalous* caustics, which are absent in systems possessing only one propagating mode. To explore the quantum-to-classical transition in electron-optical systems we calculated electron scattering from circular gated potential regions applied to multilayer rhombohedral graphene. The anomalous caustics are well visible in the wave function patterns obtained from rigorous quantum mechanical calculations in short wavelength limits. Our comprehensive study of multirefringence and anomalous caustics may inspire further works for exploring the phenomena related to multirefringent systems not only in electron optics but also in photonic crystals, acoustic materials, and magnonics.

We thank M. Berry, C. W. J. Beenakker, C. J. Lambert and Gy. Dávid for valuable discussions. This research was supported by the Ministry of Culture and Innovation and the National Research, Development and Innovation Office within the Quantum Information National Laboratory of Hungary (Grant No. 2022-2.1.1-NL-2022-00004), National Research, Development and Innovation Office (NKFIH) through Grant Nos. K134437. This project is supported by the TRILMAX Horizon Europe consortium (Grant No. 101159646).

-
- [1] M. Born, E. Wolf, and A. B. Bhatia, *Principles of Optics: Electromagnetic Theory of Propagation, Interference and Diffraction of Light*, 7th ed. (Cambridge University Press, 1999).
 - [2] E. Hecht, *Optics*, 4th ed. (Addison-Wesley, 2002).
 - [3] T. Hioki, Y. Hashimoto, and E. Saitoh, *Communications Physics* **3**, 188 (2020).
 - [4] D. R. Smith and D. Schurig, *Phys. Rev. Lett.* **90**, 077405 (2003).
 - [5] M. C. Netti, A. Harris, J. J. Baumberg, D. M. Whittaker, M. B. D. Charlton, M. E. Zoorob, and G. J. Parker, *Phys. Rev. Lett.* **86**, 1526 (2001).
 - [6] C. Díaz-Aviñó, D. Pastor, C. J. Zapata-Rodríguez, M. Naserpour, R. Kotyński, and J. J. Miret, *J. Opt. Soc. Am. B* **33**, 116 (2016).
 - [7] V. A. De Lorenci and J. P. Pereira, *Phys. Rev. A* **86**, 013801 (2012).
 - [8] V. G. Veselago, *Soviet Physics Uspekhi* **10**, 509 (1968).
 - [9] J. B. Pendry, *Phys. Rev. Lett.* **85**, 3966 (2000).
 - [10] V. M. Shalaev, W. Cai, U. K. Chettiar, H.-K. Yuan, A. K. Sarychev, V. P. Drachev, and A. V. Kildishev, *Opt Lett* **30**, 3356 (2005).
 - [11] V. M. Shalaev, *Nature Photonics* **1**, 41 (2007).
 - [12] W. Cai and V. Shalaev, *Optical Metamaterials: Fundamentals and Applications* (Springer, New York, 2010).
 - [13] M.-H. Lu, C. Zhang, L. Feng, J. Zhao, Y.-F. Chen, Y.-W. Mao, J. Zi, Y.-Y. Zhu, S.-N. Zhu, and N.-B. Ming, *Nature Materials* **6**, 744 (2007).
 - [14] V. V. Cheianov, V. Fal'ko, and B. L. Altshuler, *Science* **315**, 1252 (2007).
 - [15] J. Cserti, A. Pályi, and C. Péterfalvi, *Phys. Rev. Lett.* **99**, 246801 (2007).
 - [16] C. Péterfalvi, A. Pályi, and J. Cserti, *Phys. Rev. B* **80**, 075416 (2009).
 - [17] C. Péterfalvi, A. Pályi, Á. Ruzsnyák, J. Koltai, and J. Cserti, *Phys. Status Solidi B* **247**, 2949 (2010).
 - [18] C. G. Péterfalvi, L. Oroszlány, C. J. Lambert, and J. Cserti, *New Journal of Physics* **14**, 063028 (2012).
 - [19] J.-S. Wu and M. M. Fogler, *Phys. Rev. B* **90**, 235402 (2014).
 - [20] G.-H. Lee, G.-H. Park, and H.-J. Lee, *Nature Physics* **11**, 925 (2015).
 - [21] Y. Zhao, J. Wyrick, F. D. Natterer, J. F. Rodriguez-Nieva, C. Lewandowski, K. Watanabe, T. Taniguchi, L. S. Levitov, N. B. Zhitenev, and J. A. Stroschio, *Science* **348**, 672 (2015).
 - [22] J. M. Caridad, S. Connaughton, C. Ott, H. B. Weber, and V. Krstić, *Nature Communications* **7**, 12894 (2016).

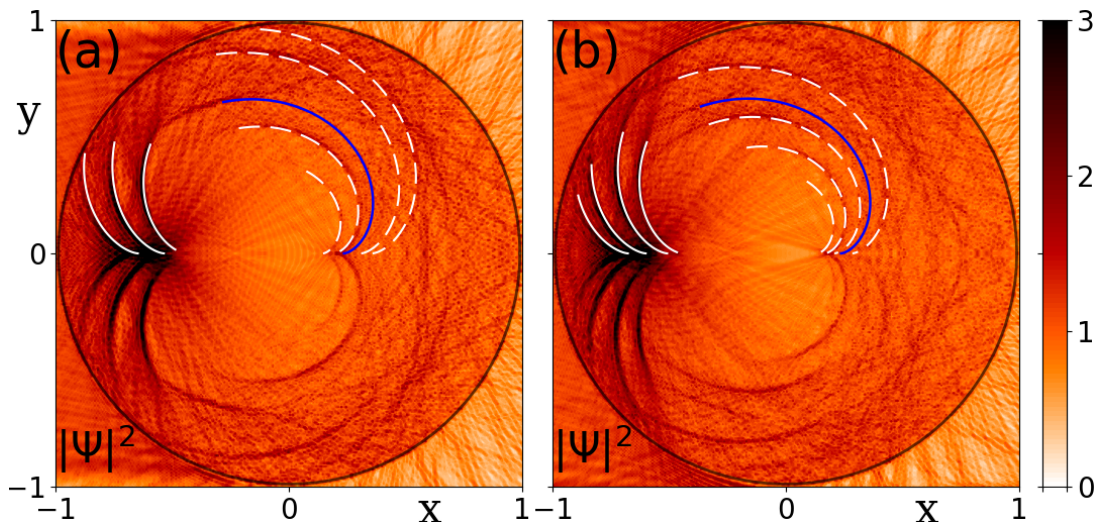


FIG. 4: The intensity of the wave function inside the circularly gated potential for ABC graphene (a) for $N = 3$ layers (b) and $N = 4$. Using Eq. (4) for $p = 1$ and $p = 2$ the regular (white and blue solid lines, respectively), and for $p = 2$ the anomalous (white dashed lines) caustic curves are plotted. The coordinates x and y are in units of R and $R = 3000a$, where a is the distance of two adjacent carbon atoms. The refractive indices of the circular regions for $N = 3$ and $N = 4$ are $\hat{n} = \{-1.25, -0.86, -0.54\}$ and $\hat{n} = \{-1.24, -0.96, -0.66, -0.48\}$, respectively.

- [23] Y. Jiang, J. Mao, D. Moldovan, M. R. Masir, G. Li, K. Watanabe, T. Taniguchi, F. M. Peeters, and E. Y. Andrei, *Nature Nanotechnology* **12**, 1045 (2017).
- [24] K.-K. Bai, J.-J. Zhou, Y.-C. Wei, J.-B. Qiao, Y.-W. Liu, H.-W. Liu, H. Jiang, and L. He, *Phys. Rev. B* **97**, 045413 (2018).
- [25] Z. Lan, N. Goldman, A. Bermudez, W. Lu, and P. Öhberg, *Phys. Rev. B* **84**, 165115 (2011).
- [26] M. M. Asmar and S. E. Ulloa, *Phys. Rev. B* **87**, 075420 (2013).
- [27] H.-Y. Xu and Y.-C. Lai, *Phys. Rev. B* **94**, 165405 (2016).
- [28] E. Andrade, R. Carrillo-Bastos, M. M. Asmar, and G. G. Naumis, *Phys. Rev. B* **106**, 195413 (2022).
- [29] A. Iurov, L. Zhemchuzhna, P. Fekete, G. Gumbs, and D. Huang, *Phys. Rev. Res.* **2**, 043245 (2020).
- [30] P. Bøggild, J. M. Caridad, C. Stampfer, G. Calogero, N. R. Papior, and M. Brandbyge, *Nature Communications* **8**, 15783 (2017).
- [31] H. Chakraborti, C. Gorini, A. Knothe, M.-H. Liu, P. Makk, F. D. Parmentier, D. Perconte, K. Richter, P. Roulleau, B. Sacépé, C. Schönenberger, and W. Yang, *Journal of Physics: Condensed Matter* **36**, 393001 (2024).
- [32] M. V. Berry and C. Upstill, Catastrophe optics: morphologies of caustics and their diffraction patterns, in *Progress in Optics XVIII*, edited by E. Wolf (North-Holland, 1980) pp. 257–346.
- [33] M. V. Berry, Singularities in waves, in *Les Houches Lecture Series Session XXXV*, edited by R. Balian, M. Kleman, and J.-P. Poirier (Amsterdam: North-Holland, 1981) pp. 453–543.
- [34] L. D. Landau, L. P. Pitaevskii, E. M. Lifshitz, and A. M. Kosevich, *Theory of Elasticity*, 3rd ed. (Butterworth-Heinemann, 1986).
- [35] J. Stoker, *Differential Geometry*, Wiley Classics Library (Wiley, 1989).
- [36] See Supplemental Material at URL-will-be-inserted-by-publisher for details of calculation.
- [37] F. Guinea, A. H. Castro Neto, and N. M. R. Peres, *Phys. Rev. B* **73**, 245426 (2006).
- [38] H. Min and A. H. MacDonald, *Progress of Theoretical Physics Supplement* **176**, 227 (2008).
- [39] S. Yuan, R. Roldán, and M. I. Katsnelson, *Phys. Rev. B* **84**, 125455 (2011).
- [40] B. V. Duppen and F. M. Peeters, *Europhysics Letters* **102**, 27001 (2013).
- [41] M. Nakamura and L. Hirasawa, *Phys. Rev. B* **77**, 045429 (2008).

Supplemental Materials: Snell's law in multirefringent systems

József Cserti,¹ Áron Holló,¹ and László Oroszlány²

¹*Department of Physics of Complex Systems, ELTE Eötvös Loránd University, H-1117 Budapest, Pázmány Péter sétány 1/A, Hungary*

²*Department of Physics of Complex Systems, ELTE Eötvös Loránd University, H-1117 Budapest, Pázmány Péter sétány 1/A, Hungary
Wigner Research Centre for Physics, H-1525, Budapest, Hungary*

SCATTERING PROBLEM FOR N LAYER RHOMBOHEDRAL GRAPHENE

Here we present the calculations of the scattering of the incident plane wave for the rhombohedral stacking (ABC) of graphene multilayer. The scattering process of the electron can be calculated by the generalization of the well-known partial wave method (see, e.g. [S1]). To this end, we take the Hamiltonian for N -layer ABC-stacked graphene multilayer around the K point (see [S2–S6]) given by

$$H_N = \begin{bmatrix} H_{\mathbf{p}} & \Gamma & 0 & \cdots & 0 \\ \Gamma^+ & H_{\mathbf{p}} & \Gamma & \cdots & 0 \\ 0 & \Gamma^+ & H_{\mathbf{p}} & \cdots & 0 \\ \vdots & \vdots & \vdots & \ddots & \Gamma \\ 0 & 0 & 0 & \Gamma^+ & H_{\mathbf{p}} \end{bmatrix} + V(\mathbf{r}) \mathbb{I}_{2N \times 2N}, \quad (\text{S1a})$$

$$H_{\mathbf{p}} = v_F \begin{bmatrix} 0 & p_- \\ p_+ & 0 \end{bmatrix}, \quad \Gamma = \begin{bmatrix} 0 & 0 \\ \gamma_1 & 0 \end{bmatrix} \quad \text{and} \quad V(\mathbf{r}) = \begin{cases} V_<, & \text{if } |\mathbf{r}| < R, \\ V_>, & \text{otherwise,} \end{cases} \quad (\text{S1b})$$

where $p_{\pm} = (p_x \pm ip_y)$ with the two-dimensional momentum operator $\mathbf{p} = (p_x, p_y) = -i\hbar\partial/\partial\mathbf{r}$, and $v_F = 3at/2\hbar$ is the Fermi velocity of the monolayer graphene, $t \approx 3$ eV is the hopping integral between the p_z orbitals of two adjacent carbon atoms and $a \approx 1.42$ Å is the carbon-carbon distance in graphene. Here $V_<$ and $V_>$ are the constant gating potentials inside ($r < R$) and outside ($r > R$) of the circular region of radius R , respectively. The Hamiltonian is given in the $2N$ component basis $(\psi_{A_1}, \psi_{B_1}, \psi_{A_2}, \psi_{B_2}, \dots, \psi_{A_N}, \psi_{B_N})$, where ψ_{A_i} (ψ_{B_i}) are the envelope functions associated with the probability amplitudes of the wave functions on sublattice A (B) of the i th layer ($i = 1, 2, \dots, N$). Finally, $\mathbb{I}_{2N \times 2N}$ is a $2N \times 2N$ unit matrix. Here, we take into account only the nearest interlayer hopping, $\gamma_1 \approx 0.4$ eV. The effective Hamiltonian for K' is obtained by exchanging p_+ and p_- .

Using the identities $[L_z, p_{\pm}] = \pm\hbar p_{\pm}$ (here $L_z = xp_y - yp_x$ is the z component of the orbital angular momentum) and the commutation relations between the Pauli matrices, it can be shown that the pseudo-angular momentum operator for N -layer ABC graphene (for trilayer see Refs. [S7, S8])

$$J_z = \mathbb{I}_{2N \times 2N} \otimes L_z + \frac{\hbar}{2} \begin{bmatrix} \sigma_0 & & & \\ & 3\sigma_0 & & \\ & & \ddots & \\ & & & (2N-1)\sigma_0 \end{bmatrix} - \frac{\hbar}{2} \mathbb{I}_{N \times N} \otimes \sigma_z, \quad (\text{S2})$$

commutes with the Hamiltonian, i.e., $[J_z, H_N] = 0$, where σ_0 is the 2×2 unit matrix and σ_z is the Pauli z matrix. Therefore, the pseudo-angular momentum is a conserved quantity in the scattering process. From now on, owing to the rotational symmetry of the Hamiltonian, it is convenient to use polar coordinates (r, φ) . Thus, to construct the eigenfunctions of the Hamiltonian (S1) we use the eigenfunction of the pseudo-angular momentum J_z , i.e.

$J_z \Psi_{k,m}(r, \varphi) = \hbar m \Psi_{k,m}(r, \varphi)$ given by

$$\Psi_{k,m}(r, \varphi) = \begin{pmatrix} C_1(k) Z_m(kr) \\ C_2(k) Z_{m+1}(kr) e^{i\varphi} \\ C_3(k) Z_{m+1}(kr) e^{i\varphi} \\ C_4(k) Z_{m+2}(kr) e^{i2\varphi} \\ C_5(k) Z_{m+2}(kr) e^{i2\varphi} \\ C_6(k) Z_{m+3}(kr) e^{i3\varphi} \\ C_7(k) Z_{m+3}(kr) e^{i3\varphi} \\ \vdots \\ C_{2N}(k) Z_{m+N}(kr) e^{iN\varphi} \end{pmatrix} e^{im\varphi}, \quad (\text{S3})$$

where $Z_m(r)$ stands for the first-kind $J_m(r)$ and second-kind $Y_m(r)$ Bessel functions, and for the Hankel functions of the first kind $H_m^{(1)}(r)$ and second kind $H_m^{(2)}(r)$ (here $m \in \mathbb{Z}$). For a given wave number k the complex eigenvector $\mathbf{C}(k) = [C_1(k), C_2(k), \dots, C_{2N}(k)]^T$ can be obtained from the Schrödinger equation $H_N \Psi_{k,m}(r, \varphi) = E(k) \Psi_{k,m}(r, \varphi)$ by substituting here the wave function (S3) resulting in the following eigenvalue equation for $\mathbf{C}(k)$:

$$[\hbar v_F k \Sigma + \mathcal{A} + V_{\leq} \mathbb{I}_{2N \times 2N}] \mathbf{C}(k) = E(k) \mathbf{C}(k), \quad \text{where} \quad (\text{S4a})$$

$$\Sigma = \mathbb{I}_{N \times N} \otimes \sigma_y, \quad \mathcal{A} = \begin{pmatrix} 0 & \Gamma & 0 & 0 & \cdots & 0 \\ \Gamma^+ & 0 & \Gamma & 0 & \cdots & 0 \\ 0 & \Gamma^+ & 0 & \Gamma & \cdots & 0 \\ \vdots & \vdots & \vdots & \vdots & \ddots & 0 \\ 0 & 0 & \cdots & \Gamma^+ & 0 & \Gamma \end{pmatrix}. \quad (\text{S4b})$$

To obtain Eq. (S4) we used the following relation

$$p_{\pm} Z_m(kr) e^{im\varphi} = \pm i \hbar k Z_{m \pm 1}(kr) e^{i(m \pm 1)\varphi}, \quad (\text{S5a})$$

where the momentum operator and the orbital angular momentum operator in polar coordinates are given by

$$p_{\pm} = -i \hbar e^{\pm i\varphi} \left[\frac{\partial}{\partial r} \pm \frac{i}{r} \frac{\partial}{\partial \varphi} \right] \quad \text{and} \quad L_z = -i \hbar \partial_{\varphi}. \quad (\text{S5b})$$

As an example, Fig. S1 shows the dispersion relations $E(k)$ inside ($r < R$) and outside ($r > R$) of the circular region. The energy E of the incoming electron propagates from the left to the right direction with wave number k_0 . The gating potential inside the circular region is a constant value of $V_{<}$ and zero outside. Inside the circular region, the allowed wave numbers with energy E are $k_1^<$, $k_2^<$ and $k_3^<$. We set the value of $V_{<}$ in such a way that $\mathbf{v}(\mathbf{k}) \cdot \mathbf{k} < 0$ for the group velocities $\mathbf{v}(\mathbf{k})$ at the energy E , resulting in negative refraction indices.

In the scattering problem, the energy of the incident electron is given and we need to determine the allowed wave numbers corresponding to the propagating modes. However, from the eigenvalue equation (S4), we obtain only the energy $E(k)$ as a function of wave number k . The inverse problem, namely, calculating the allowed wave number k for a given energy E is generally a difficult numerical problem involving the root finding. Fortunately, in our case, after rearranging Eq. (S4a) the wave number k for a given energy E can be determined from the eigenvalue equation of the matrix $\Lambda(E)$ as a convenient and standard procedure numerically:

$$\Lambda(E) \mathbf{C}(k) = \hbar v_F k \mathbf{C}(k), \quad \text{where} \quad (\text{S6a})$$

$$\Lambda(E) = -\Sigma [\mathcal{A} + (V_{\leq} - E) \mathbb{I}_{2N \times 2N}]. \quad (\text{S6b})$$

Moreover, at the same time, we also obtained the $2N$ component vector \mathbf{C} in the wave function given by Eq. (S3). Note that $\Sigma^{-1} = \Sigma$. In the above eigenvalue equation, there are $2N$ different numbers of the eigenvalues k_{ν} labeled by mode $\nu = 1, 2, \dots, 2N$. Note that some of the eigenvalues can be complex numbers. For the case of complex wave numbers, we should choose the one for which the partial cylindrical wave function tends to zero asymptotically.

The scattering of the incident electron can be calculated by the generalization of the well-known partial wave method (see, e.g., [S1]). To this end, we construct the wave function inside and outside of the circular region as

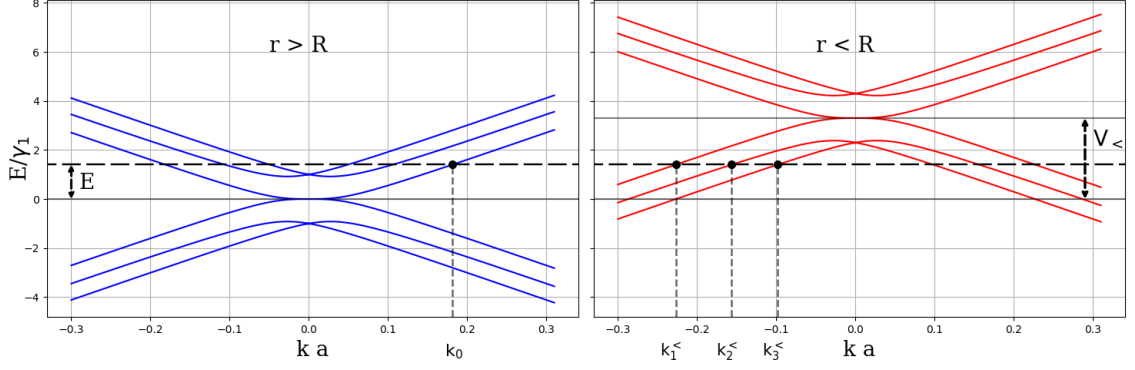


FIG. S1: The energy dispersion $E(k)$ (in units of γ_1) as functions of the wave number k outside (left panel) and inside (right panel) of the circular region in the case of $N = 3$ layers. We take the gate potentials $V_< = 3.3\gamma_1$ and $V_> = 0$, and $R = 3000a$ in our numerical calculation. The energy of the incoming electron is $E = 1.4\gamma_1$ from which the calculated wave numbers are $k_0a = 0.181$ for $r > R$, and $k_1^<a = -0.227, k_2^<a = -0.156, k_3^<a = -0.098$ for $r < R$. Thus, from Eq. (3) of the main text the refractive indices are $\hat{n} = \{-1.25, -0.86, -0.54\}$.

a linear combination of the eigenfunctions given by Eq. (S3). We assume that the wave number of the inward-propagating partial wave is k_ν , corresponding to mode ν . This is the ν th solution of the equation $E(k_\nu) = E$, which is equivalent to the eigenvalues of Eq. (S6). In the scattering problem, we choose k_ν as a real number. Then the wave function outside the circular region ($r > R$) can be written as

$$\Psi_{m,\nu}^>(r, \varphi) = \mathbf{h}_{m,\nu}^{(2)} + \sum_{\beta=1}^N S_{\nu\beta} \mathbf{h}_{m,\beta}^{(1)}, \quad \text{for } r > R, \quad (\text{S7a})$$

where

$$\mathbf{h}^{(d)}(r, \varphi) = \begin{pmatrix} C_1^>(k_\nu) H_m^{(d)}(k_\nu r) \\ C_2^>(k_\nu) H_{m+1}^{(d)}(k_\nu r) e^{i\varphi} \\ C_3^>(k_\nu) H_{m+1}^{(d)}(k_\nu r) e^{i\varphi} \\ C_4^>(k_\nu) H_{m+2}^{(d)}(k_\nu r) e^{i2\varphi} \\ C_5^>(k_\nu) H_{m+2}^{(d)}(k_\nu r) e^{i2\varphi} \\ C_6^>(k_\nu) H_{m+3}^{(d)}(k_\nu r) e^{i3\varphi} \\ C_7^>(k_\nu) H_{m+3}^{(d)}(k_\nu r) e^{i3\varphi} \\ \vdots \\ C_{2N}^>(k_\nu) H_{m+N}^{(d)}(k_\nu r) e^{iN\varphi} \end{pmatrix} e^{im\varphi}, \quad (\text{S7b})$$

and $\mathbf{h}^{(1)}$ and $\mathbf{h}^{(2)}$ are built up from the inward- and outward-propagating cylindrical waves, respectively, while $\mathbf{C}^>(k_\nu)$ is the eigenvector in Eq. (S6) with potential $V_>$, and $S_{\nu\beta}$ is the scattering matrix of the partial waves from wave number k_ν to k_β . Note that $E(k_\nu) = E(k_\beta) = E$. The scattering matrix $S_{\nu\beta}$ describes the scattering of a single incoming partial cylindrical wave $\mathbf{h}_{m,\beta}^{(1)}$ and can be obtained from the boundary condition of the wave function at $r = R$ (will be discussed below).

The wave function inside the circular potential region ($0 < r < R$) should be built up from the partial waves (S3) with the Bessel functions which is non-singular at $r = 0$:

$$\Psi_{m,\nu}^<(r, \varphi) = \sum_{\mu=1}^N A_\mu \mathbf{J}_{m,\mu}, \quad (\text{S8a})$$

where

$$\mathbf{J}_{m,\mu}(r, \varphi) = \begin{pmatrix} C_1^<(k_\mu)J_m(k_\mu r) \\ C_2^<(k_\mu)J_{m+1}(k_\mu r)e^{i\varphi} \\ C_3^<(k_\mu)J_{m+1}(k_\mu r)e^{i\varphi} \\ C_4^<(k_\mu)J_{m+2}(k_\mu r)e^{i2\varphi} \\ C_5^<(k_\mu)J_{m+2}(k_\mu r)e^{i2\varphi} \\ C_6^<(k_\mu)J_{m+3}(k_\mu r)e^{i3\varphi} \\ C_7^<(k_\mu)J_{m+3}(k_\mu r)e^{i3\varphi} \\ \vdots \\ C_{2N}^<(k_\mu)J_{m+N}(k_\mu r)e^{iN\varphi} \end{pmatrix} e^{im\varphi}, \quad (\text{S8b})$$

where $\mathbf{C}^<(k_\mu)$ is the eigenvector in Eq. (S6) with potential $V_<$ for wave number k_μ satisfying $E(k_\mu) = E$.

Finally, the scattering matrix $S_{\nu\beta}$ and the amplitude A_μ are determined from the boundary conditions, i.e., the continuity of the total wave function: $\Psi_{m,\nu}^>(r = R, \varphi) = \Psi_{m,\nu}^<(r = R, \varphi)$, which leads to the following inhomogeneous linear equation system for a given m and mode ν :

$$\sum_{\mu=1}^N A_\mu \mathbf{J}_{m,\mu} = \mathbf{h}_{m,\nu}^{(2)} + \sum_{\beta=1}^N S_{\nu\beta} \mathbf{h}_{m,\beta}^{(1)}, \quad (\text{S9})$$

where the functions $\mathbf{J}_{m,\mu}$, $\mathbf{h}_{m,\nu}^{(1)}$ and $\mathbf{h}_{m,\nu}^{(2)}$ are evaluated at $r = R$. Note that the φ dependence is dropped out from this equation. This system of equations has $2N$ number of equations with N number of unknown amplitude A_ν and scattering matrix element $S_{\nu\beta}$.

We now consider the scattering of an incident plane wave propagating along the x direction for $r > R$. Using Eq. (S4) one can show that such an eigenstate Φ_ν with a given energy E and wave number k_ν is given by

$$\Phi_\nu = e^{ik_\nu x} \begin{pmatrix} C_1^>(k_\nu) \\ i^{-1} C_2^>(k_\nu) \\ i^{-1} C_3^>(k_\nu) \\ i^{-2} C_4^>(k_\nu) \\ i^{-2} C_5^>(k_\nu) \\ i^{-3} C_6^>(k_\nu) \\ i^{-3} C_7^>(k_\nu) \\ \vdots \\ i^{-N} C_{2N}^>(k_\nu) \end{pmatrix}, \quad (\text{S10})$$

where the vector $\mathbf{C}^>(k_\nu)$ is the eigenvector in Eq. (S6) with potential $V_>$. Then from the Jacobi–Anger expansion [S9, S10]

$$e^{ikr \cos \varphi} = \sum_{m=-\infty}^{\infty} i^m J_m(kr) e^{im\varphi}, \quad (\text{S11})$$

it can be shown that the plane wave Φ_ν can be written as a linear combination of incoming and outgoing cylindrical waves:

$$\Phi_\nu = \sum_{m=-\infty}^{\infty} \frac{i^m}{2} \left(\mathbf{h}_{m,\nu}^{(1)} + \mathbf{h}_{m,\nu}^{(2)} \right). \quad (\text{S12})$$

This expansion allows us to use the scattering matrix $S_{\nu\beta}$ and the amplitude A_μ determined from Eq. (S9) to derive the wave function describing the scattering of the plane wave. Then inside and outside of the circular region the wave functions $\Psi_\nu^<$ and $\Psi_\nu^>$ become

$$\Psi_\nu^<(r, \varphi) = \sum_{m=-\infty}^{\infty} \sum_{\mu=1}^N \frac{i^m}{2} A_\mu \mathbf{J}_{m,\mu}, \quad \text{for } r < R, \quad (\text{S13a})$$

$$\Psi_\nu^>(r, \varphi) = \Phi_\nu + \sum_{m=-\infty}^{\infty} \sum_{\beta=1}^N \frac{i^m}{2} (S_{\nu\beta} - \delta_{\nu\beta}) \mathbf{h}_{m,\beta}^{(1)}, \quad \text{for } r > R. \quad (\text{S13b})$$

The second term in (S13b) is the scattered wave due to the scattering of the incident plane wave on the scattering region described by the potential $V(\mathbf{r})$.

BIREFRINGENCE IN BILAYER GRAPHENE AND THE EMERGENCE OF ANOMALOUS CAUSTICS

Figure S2 shows the dispersion relations $E(k)$ inside ($r < R$) and outside ($r > R$) of the circular region. The energy E of the incoming electron propagates from the left to the right direction with wave number k_0 . The gating potential inside the circular region is a constant value of $V_<$ and zero outside. Inside the circular region, the allowed wave numbers with energy E are $k_1^<$, $k_2^<$ and $k_3^<$. We set the value of $V_<$ in such a way that $\mathbf{v}(\mathbf{k}) \cdot \mathbf{k} < 0$ for the group velocities $\mathbf{v}(\mathbf{k})$ at the energy E , resulting in negative refraction indices.

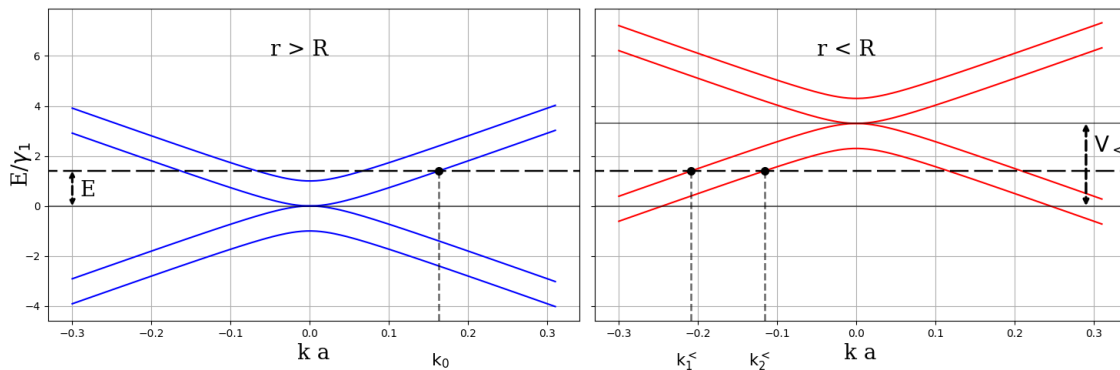


FIG. S2: The energy dispersion $E(k)$ (in units of γ_1) as functions of the wave number k outside (left panel) and inside (right panel) of the circular region in the case of $N = 2$ layers. We take the gate potentials $V_< = 3.3\gamma_1$ and $V_> = 0$ in our numerical calculation. The energy of the incoming electron is $E = 1.4\gamma_1$ from which the calculated wave numbers are $k_0 a = 0.163$ for $r > R$, and $k_1^< a = -0.209$, $k_2^< a = -0.116$ for $r < R$. Thus, from Eq. (3) of the main text the refractive indices are $\hat{n} = \{-1.28, -0.71\}$.

Figure S3 shows the scattered wave function pattern inside the circular region for the case of $N = 2$ layers. Using Eq. (5) of the main text we also plotted the regular caustics for $p = 1$ and $p = 2$ chords (solid lines in Fig. S3a), and the anomalous caustics for $p = 2$ chords (dashed lines in Fig. S3b). It can be seen from the figure that these curves agree well with the wave function pattern intensity maxima obtained from the full quantum mechanical scattering calculations.

$x_{\text{cusp}}^{(p=1)}$	$n_1 \rightarrow n_2$	$x_{\text{cusp}}^{(p=2)}$
-0.44	-0.71 \rightarrow -1.28	0.17
-0.58	-1.28 \rightarrow -1.28	0.23
-	-0.71 \rightarrow -0.71	0.27
-	-1.28 \rightarrow -0.71	0.35

TABLE I: The locations of the cusps $x_{\text{cusp}}^{(p=1)}$ for $p = 1$ chords, and $x_{\text{cusp}}^{(p=2)}$ for $p = 2$ chords of the caustic curves shown in Fig. S3 in case of $N = 2$ layers. The locations are in units of R . For $p = 1$ there are only regular caustic curves. In the case of $p = 2$ the two refractive indices n_1 and n_2 are the same for regular caustics, while for different n_1 and n_2 the caustics are anomalous (red numbers).

From Eq. (3) of the main text with the allowed wave numbers for a given energy (see the caption of Fig. S3) the two refractive indices of the circular regions are $\hat{n} = \{-1.28, -0.71\}$. Then from Eq. (6) of the main text we find $x_{\text{cusp}}^{(1)} = -0.44R$, and $x_{\text{cusp}}^{(1)} = -0.58R$, $x_{\text{cusp}}^{(2)} = 0.23R$, and $x_{\text{cusp}}^{(2)} = 0.27R$, while for anomalous caustics from Eq. (7) of the main text we have $x_{\text{cusp}}^{(2)} = 0.17R$, and $x_{\text{cusp}}^{(2)} = 0.35R$. In Fig. S3 one can see that the positions of these cusps also agree very well with that obtained from the exact quantum calculations.

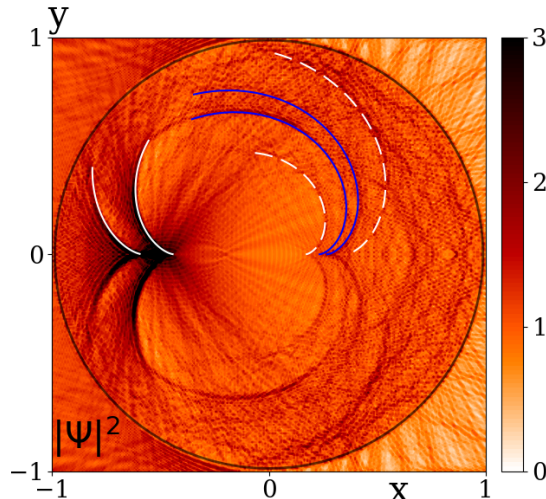


FIG. S3: The intensity of the wave function inside the circular region for ABC graphene with $N = 2$ layers. The intensity of the wave function inside the circularly gated potential for ABC graphene (a) for $N = 3$ layers (b) and $N = 4$. Using Eq. (5) of the main text for $p = 1$ and $p = 2$ the regular (white and blue solid lines, respectively), and for $p = 2$ the anomalous (white dashed lines) caustic curves are plotted. The coordinates x and y are in units of R and $R = 3000a$, where a is the distance of two adjacent carbon atoms. To have a better view, only half-sections of the symmetric caustic curves are shown.

GENERAL EQUATION FOR THE CAUSTICS OF STRAIGHT LINES

Here we derive the equation for the caustics, i.e., the envelope of the family of straight lines in two dimensions. The equation of the family of straight lines depending on a parameter α can be given by

$$[\mathbf{r} - \mathbf{r}_0(\alpha)] \cdot \mathbf{n}(\alpha) = 0, \quad (\text{S14})$$

where $\mathbf{r}_0(\alpha)$ is a point on the line and $\mathbf{n}(\alpha)$ is the normal vector to the line (not necessarily a unit vector) for a given parameter α . Now, differentiating Eq. (S14) with respect to α we obtain

$$\mathbf{r} \cdot \dot{\mathbf{n}} = \dot{\mathbf{r}}_0 \cdot \mathbf{n} + \mathbf{r}_0 \cdot \dot{\mathbf{n}}. \quad (\text{S15})$$

Here the dot denotes the derivative with respect to α . The solution of Eqs. (S14) and (S15) for \mathbf{r} gives the parametric equation of the caustics curve $\mathbf{r}_c(\alpha)$. To solve these two equations we are looking for the solution in the following form:

$$\mathbf{r} = \mathbf{r}_0 + C \mathbf{v}, \quad (\text{S16})$$

where the vector \mathbf{v} and the real number C are to be determined. Substituting this form into Eqs. (S14) and (S15) we find

$$C \mathbf{v} \cdot \mathbf{n} = 0 \quad \text{and} \quad C \mathbf{v} \cdot \dot{\mathbf{n}} = \dot{\mathbf{r}}_0 \cdot \mathbf{n}. \quad (\text{S17})$$

For finite C the first equation can be satisfied when \mathbf{v} is perpendicular to \mathbf{n} , i.e., $\mathbf{v} \cdot \mathbf{n} = 0$. In two dimensions the vector \mathbf{v} should be the direction vector of the straight line. While the second equation gives the solution for C , namely $C = (\dot{\mathbf{r}}_0 \cdot \mathbf{n}) / (\mathbf{v} \cdot \dot{\mathbf{n}})$. Then, using Eq. (S16) the parametric equation of the caustics curve is

$$\mathbf{r}_c(\alpha) \equiv \mathbf{r} = \mathbf{r}_0 + \frac{\dot{\mathbf{r}}_0 \cdot \mathbf{n}}{\mathbf{v} \cdot \dot{\mathbf{n}}} \mathbf{v}, \quad (\text{S18})$$

where \mathbf{r}_0 is a given point on the straight line, \mathbf{v} and \mathbf{n} are the direction and the normal vector of the straight line, respectively. All vectors depend on the parameter α . Note that if \mathbf{n} is normalized then in two dimensions \mathbf{v} is parallel to $\dot{\mathbf{n}}$ thus it can be replaced by $\dot{\mathbf{n}}$ in Eq. (S18). However, due to the normalization of \mathbf{n} , in general, this approach is less suitable for analytical calculations. Equation (S18) is the general equation for the caustic curve of the family of straight lines given by Eq. (S14).

APPLICATION OF THE GENERAL EQUATION FOR A FAMILY OF CHORDS IN A CIRCLE

Assume that the two endpoints of a chord in a circle with unit radius are given by

$$\mathbf{r}_A = \begin{bmatrix} \cos \varphi_A \\ \sin \varphi_A \end{bmatrix}, \quad \mathbf{r}_B = \begin{bmatrix} \cos \varphi_B \\ \sin \varphi_B \end{bmatrix}, \quad (\text{S19})$$

where φ_A and φ_B depending on the parameter α are the polar angle of the vectors \mathbf{r}_A and \mathbf{r}_B . The direction vector \mathbf{v} and the normal vector \mathbf{n} of the chords are

$$\mathbf{v} = \mathbf{r}_B - \mathbf{r}_A = \begin{bmatrix} \cos \varphi_B - \cos \varphi_A \\ \sin \varphi_B - \sin \varphi_A \end{bmatrix}, \quad \mathbf{n} = \begin{bmatrix} -(\sin \varphi_B - \sin \varphi_A) \\ \cos \varphi_B - \cos \varphi_A \end{bmatrix}. \quad (\text{S20})$$

Here $\mathbf{v} \cdot \mathbf{n} = 0$.

The derivatives of \mathbf{r}_A and \mathbf{n} with respect to the parameter α are

$$\dot{\mathbf{r}}_A = \begin{bmatrix} -\sin \varphi_A \\ \cos \varphi_A \end{bmatrix} \dot{\varphi}_A, \quad \dot{\mathbf{n}} = -\begin{bmatrix} \cos \varphi_B \\ \sin \varphi_B \end{bmatrix} \dot{\varphi}_B + \begin{bmatrix} \cos \varphi_A \\ \sin \varphi_A \end{bmatrix} \dot{\varphi}_A. \quad (\text{S21})$$

Using the general equation (S18) for the caustics curve and with $\mathbf{r}_0 = \mathbf{r}_A$ we find

$$\mathbf{r}_c(\alpha) = \frac{\mathbf{r}_A \dot{\varphi}_B + \mathbf{r}_B \dot{\varphi}_A}{\dot{\varphi}_A + \dot{\varphi}_B}. \quad (\text{S22})$$

-
- [S1] F. Schwabl, *Quantum Mechanics* (Springer-Verlag Berlin Heidelberg, 1992).
[S2] F. Guinea, A. H. Castro Neto, and N. M. R. Peres, *Phys. Rev. B* **73**, 245426 (2006).
[S3] H. Min and A. H. MacDonald, *Progress of Theoretical Physics Supplement* **176**, 227 (2008).
[S4] S. Yuan, R. Roldán, and M. I. Katsnelson, *Phys. Rev. B* **84**, 125455 (2011).
[S5] B. V. Duppen and F. M. Peeters, *Europhysics Letters* **102**, 27001 (2013).
[S6] M. Nakamura and L. Hirasawa, *Phys. Rev. B* **77**, 045429 (2008).
[S7] M. Mirzakhani, M. Zarenia, P. Vasilopoulos, and F. M. Peeters, *Phys. Rev. B* **95**, 155434 (2017).
[S8] H. Xiong, W. Jiang, Y. Song, and L. Duan, *Journal of Physics: Condensed Matter* **29**, 215002 (2017).
[S9] M. Abramowitz and I. Stegun, *Handbook of Mathematical Functions*, 9th ed. (Dover Publication Inc., New York, NY, 1972).
[S10] I. S. Gradshteyn and I. M. Ryzhik, *Table of integrals, series, and products*, 7th ed. (Elsevier/Academic Press, Amsterdam, 2007).